
OH CONCENTRATION PROFILES OVER ALUMINA, QUARTZ, AND PLATINUM SURFACES USING LASER-INDUCED FLUORESCENCE SPECTROSCOPY IN LOW-PRESSURE HYDROGEN/OXYGEN FLAMES

**SHAURYA PRAKASH
NICK G. GLUMAC
N. SHANKAR
MARK A. SHANNON***

Department of Mechanical and Industrial Engineering,
University of Illinois at Urbana-Champaign, Urbana,
Illinois, USA

Laser-induced fluorescence measurements of OH radical concentration are performed in the post-flame gaseous region of a stoichiometric H₂/O₂ mixture combusting at 20 Torr. The measurements are taken near surfaces of three different materials [α -alumina (Al₂O₃), quartz (SiO₂), and platinum (Pt) on alumina] at different surface temperatures (from ~700 to 1100 K). A comparative analysis of some of the factors affecting OH recombination rate are provided as a function of material and temperature. Of the samples tested, Al₂O₃ is observed to be the least active whereas Pt on Al₂O₃ is the most active, with SiO₂ at an intermediate level with respect to OH recombination rate on surfaces indicating a quantitative difference between the two relatively inert materials. The result of these

Received 3 May 2004; accepted 14 October 2004.

The current work was supported by the Department of Defense Multidisciplinary University Research Initiative (MURI) program administered by the Army Research Office under grant DAAD19-01-1-0582. Material characterization was carried out at the Center for Microanalysis of Materials, University of Illinois, which is partially supported by the U.S. Department of Energy under grant DEFG02-91-ER45439.

*Address correspondence to mshannon@uiuc.edu

differences in recombination rates is that the overall OH number density in the gaseous region within millimeters of the surface was observed to differ by over one order of magnitude between Pt and Al₂O₃ under nearly identical conditions.

Keywords: radical, recombination, LIF, OH, combustion, Pt, Al₂O₃, SiO₂

INTRODUCTION

The high energy and power densities often achieved with combustion-based heat engines may provide significant advantages over traditional small-scale power sources such as batteries, *if* the heat energy can be efficiently generated and converted to a usable form at a very small scale. For instance, hydrocarbon fuels can provide 40–50 MJ/kg of heat energy, compared to 0.4–0.7 MJ/kg of electrical energy for state-of-the art Li-ion batteries (Fernandez-Pello, 2002; Kelley et al., 2002; Vican et al., 2002), and much lower energy densities of pressurized fluids used for micro-thrusters. Even a 2% conversion of that heat energy to usable energy (giving 0.8 to 1 MJ/kg) will exceed the best battery energy densities currently achieved, and conversion efficiencies greater than 20% would increase performance by more than an order of magnitude. Thus, there has been a growing interest in developing efficient micro- to miniature combustion-powered heat engines to convert the high chemical energy density of hydrocarbon fuels to electrical power, or to thrust for jets and micro-rockets. The problem being faced by micro-miniature heat engines is that, as the size is reduced, the surface-area-to-volume ratio of the combustor begins to dominate the combustion process. Both the chemical reactivity of the wall and the heat transfer to the wall affect the radical recombination and generation rates of the reactants. If important radicals such as hydroxyl or methyl are destroyed at or near the wall too quickly, the combustion process can be quenched. The thermal and chemical quenching pathways are strongly coupled, so that very small changes in temperature or chemical activity of the wall can lead to significant changes in radical concentration near the wall, making gas-phase combustion using air as the oxidant difficult to sustain below a critical length scale (i.e. quenching distance) of a few millimeters (Kuo, 1986). Recently, however, it was observed that hydrogen and hydrocarbon (methane, propane, acetylene) flames can be stable in combustor cavities much smaller than 1 mm in critical length scale, provided

the walls are well above 500°C and are made from silica (SiO_2) and/or alumina (Al_2O_3), as demonstrated in microcombustors developed by Masel and Shannon (2001) and reported by Raimondeau et al. (2002) and Miesse et al. (2004). Gas-phase flames could not be sustained at any wall temperature for metallic and carbide microcombustors with critical lengths less than about 2.5 mm, nor for microcombustors made from the aluminosilicate family of materials at temperatures lower than about $450\text{--}500^\circ\text{C}$. The hypothesis for why sustained combustion occurs for higher-temperature combustor walls made of aluminum and silicon oxides is that these conditions make the walls less reactive, so that the concentration of important radicals such as OH within the gas above the surface does not decrease to a level sufficient to inhibit gas-phase combustion. The radical concentration in the gas-phase may increase if these wall materials slow the radical recombination rates at the wall and/or help generate more radicals due to reactions with other species at the hot wall, such as water. However, there is as yet no *direct evidence* that has been reported that the combination of these wall compositions and temperatures strongly affect the concentration of radicals near the wall and into the combustor volume.

Since the hydroxyl (OH) radical is an important species for stabilizing and sustaining gas-phase combustion for hydrogen and hydrocarbon fuels, this paper reports on the concentration of the OH radical as a function of wall material and temperature in a low-pressure stoichiometric hydrogen/oxygen premixed flame. The experiments investigate, at temperatures ranging from 730 to 1063 K, the effect of wall materials generally considered to be highly catalytic and reactive (Pt) for hydrogen and oxygen combustion systems, to those often considered non-catalytic and relatively inert (quartz and α -alumina). The low-pressure regime is chosen because the hydrodynamic boundary layer (δ_h) and flame zone (δ_{fz}) both widen at lower pressures, allowing the laser-induced fluorescence (LIF) diagnostic tool to more accurately map the OH profile. This wider, low-pressure concentration profile should also be qualitatively similar to the narrower sub-millimeter profile that is more typical for microcombustors operating at higher pressures. The main purpose of this paper is to show that the wall composition and surface temperature can affect the OH concentration profile throughout the entire boundary layer by over an order of magnitude, thereby supporting the initial hypothesis that reducing the chemical reactivity of the wall material and increasing the wall temperature can

suppress wall quenching of flames in combustors with critical length in the submillimeter regime.

A large amount of work has been conducted on the hydrogen/oxygen flame and the OH radical concentration profiles near catalytic surfaces, primarily Pt and Pd. Furthermore, extensive literature exists on LIF spectroscopic studies, such as the work by Daily (1997) and Laurendeau and Goldsmith (1989), and the structure, behavior, and mechanisms of the hydrocarbon- and hydrogen/oxygen flames, such as the work presented by Miller and Bowman (1989) in their review article. The influence of surfaces on the quenching of flames and on supporting heterogeneous catalytic combustion has generated a significant amount of interest in flame-wall interactions and their effect on potential applications (Fridell and Rasen, 1994; Kurkov and Mirsky, 1968; Kyritsis et al., 2002; Marsden and Linnett, 1995; Reinke et al., 2002; Scwieder-noch et al., 2002; Sidwell et al., 2002; Takeda et al., 2002).

The authors chose to measure the OH concentration near walls in a stagnation flow reactor for several reasons. The geometry is nearly one-dimensional with an impinging flow and is accessible for probing with laser diagnostics to obtain spatial profiles of key species. Several researchers, including Khadiya and Glumac (2000), Aghalayam et al. (1998), Hahn et al. (1996), and Deutschmann et al. (1996), have also exploited the choice of the stagnation flow geometry for a variety of experimental and computational combustion studies and related applications. In addition, the wide database of knowledge with respect to catalytic surfaces such as Pt provides a good baseline experimental reference for this work. Some of the notable studies on the influence of catalytic surfaces in stagnation flow configuration on both gas-phase and surface combustion, including those by Forsth et al. (1999), Ikeda et al. (1995), Warnatz et al. (1994) and Ljungstrom et al. (1987), present several important characteristics of combustion on catalytic surfaces, including a comparison between some of the commonly used catalysts. Detailed work by Gudmundson et al. (1998), Balat et al. (1997), Ikeda et al. (1995), Warnatz et al. (1994), and Miller and Bowman (1989) provide detailed mechanisms for both gas-phase and surface-chemistry models. These models provide likely chemical reactions with thermo-chemical data and describe many of the issues involved in the stagnation flow combustion problem on a reactive surface such as Pt.

A key question that has been addressed in these previous studies is the effect that recombination at the wall has on combustion species.

In particular, it has been shown that for a given set of inlet conditions the post-flame measurement of OH radical concentration varies essentially only by changes in wall conditions. Therefore, post-flame measurements are expected to elucidate the effect of OH-wall interactions separately from the complexities of the strongly coupled generation and recombination of OH that occurs within the flame zone itself.

Although several researchers have studied flame characteristics, flame behavior, and the effect of catalytic surfaces on combustion processes, the knowledge base detailing and quantifying the effect of wall material and surface temperature on the quenching of the OH radical near different types of relatively inert surfaces is still limited. This current work reports on the OH concentration in the gas phase for three basic types of surfaces: Pt, quartz, and alumina at wall temperatures from ~ 700 to 1100 K. The manner in which the surfaces are prepared (lapping, polishing, and/or annealing the substrates) is also varied to report on the effect that small differences in fine surface morphology have on the OH concentration profile. This work is a phenomenological study quantifying the effect of wall material and overall surface conditions on the OH radical recombination at a surface. The results show that quartz and α -alumina wall materials are the most likely to raise, and Pt surfaces are the most likely to reduce, the OH radical concentration in the post-flame gas region near the wall. In addition, the surface temperature has a strong effect on the OH concentration, and the degree to which OH concentration increases with temperature also strongly depends on the surface composition.

EXPERIMENTAL

Design of Experiment and Experimental Apparatus

In this paper, a comparison is made of OH profiles over targets made of Pt on alumina, pure α - Al_2O_3 (polycrystalline α -alumina), and SiO_2 (quartz). Post-flame gases from a stoichiometric H_2/O_2 flame impinge on the substrate walls with a stagnation flow, and LIF spectroscopy is used to measure the OH radical concentration profile. The LIF data are converted to OH number density, as discussed later. The experimental setup is a commonly used LIF experimental facility (Glumac, 1997; Khadiya and Glumac, 2000; Rensberger et al., 1989) consisting of a vacuum combustion chamber, lasers, coupling optics, and an optoelectronic imaging system for signal detection. The details on the

experimental setup can be found in the work by Khadiya and Glumac (2000) and Glumac (1997); however, a brief description follows.

The experimental combustion chamber consists of a water-cooled flat-flame burner and heated substrate holder, and a high-conductance vacuum system with four view ports for observation and optical access. The flat-flame burner (60 mm diameter) and the substrate holder assembly are supported within the vacuum chamber. The substrate is maintained at a fixed distance of 20 mm from the burner face. A manually operated translation stage allows the position of the burner and substrate to be moved together with respect to the horizontal and to be controlled within 0.03 mm. The substrate assembly consists of a base to hold the substrate in a specially designed ceramic holder, radiation shields around the base and substrate to mitigate heat loss, and a resistive heater placed under the substrate. A thermocouple (TC) is attached to the back of the substrate with a ceramic adhesive (Cotronics 989). A temperature calibration experiment was conducted to correlate the top surface temperature, of interest in these experiments, to the bottom surface temperature being measured. The pressure in the chamber is monitored by a capacitance manometer and is maintained at 20 Torr. The pressure is maintained within 0.1 Torr of the set point by a throttle valve and an electronic valve controller. A premixed stoichiometric H_2/O_2 flat flame is obtained with a total mass flux of $1.0 \text{ g/cm}^2/\text{s}$ controlled by MKS model 1179 A mass flow controllers.

A total of eight types of substrates were chosen for this study. Two of the substrates had Pt films evaporated on two different backing surfaces. One backing surface was an as-received sintered high-purity (99.5%) polycrystalline α -alumina disc 3 mm thick with an average surface roughness, R_a , of $4 \mu\text{m}$, and the second was the same type of α -alumina disc polished with diamond grit to an R_a of $0.14 \mu\text{m}$. Four other substrates were the α -alumina disks that were (1) polished; (2) polished and annealed; (3) as-received from the manufacturer, Superior Tech Ceramics; and (4) as-received and annealed. A similar set of two polished, and polished and annealed, substrates for quartz were also used. These substrate materials were chosen to address specific questions with regard to the effect of material and surface conditions on the rate of OH destruction near each of the substrate walls.

A 500 mm focal length lens is used to focus the laser-beam into the combustion chamber. The fluorescence signal is collected perpendicular to the irradiating beam to increase the spatial resolution as suggested by

Daily (1997). The collection optics consist of two fused silica lenses with 150 and 200 mm focal lengths. There are two collection lenses, one inside the chamber and one outside, that focus the fluorescent signal to the monochromator slit.

A Spectra Physics GCR-150 Nd:YAG laser pumps a Lumonics Spectrum Master HD-300 dye laser. The dye laser output is 562 nm and is frequency doubled by a Beta Barium Borate (BBO) crystal to produce a 281 nm output. The fluorescence is collected using a 150 mm monochromator with a 0.5-mm entrance slit and a 5 mm exit slit. The resulting bandpass of the order of 28 nm covers a major portion of the (0,0) and (1,1) bands.

The fluorescence signal after collection is passed through a Hamamatsu 3177-51 photomultiplier tube (PMT) and the output is then amplified 25 times. The amplified signal generated by the PMT is sent to a Le Croy 9360 digital oscilloscope to average the signal over a prescribed detection gate.

Experimental Procedure

A wavelength band of 283.3330–283.3430 nm is used to excite the (1,0) band of the OH radical of the $A^2\Sigma^+ \rightarrow X^2\Pi$ transition. It has been shown previously (Rensberger et al., 1989) that in low-pressure LIF setups with prompt detection gate quenching effects can be minimized; thus, with respect to quenching of OH, the choice of the particular transition is not important. The particular transition studied for the diagnostic study was $Q_{12}(6)$. The Boltzmann thermal emission fraction of the $F_2(6)$ level varies by a maximum of 10% for the temperature range under consideration (700–1100 K), which is corrected for as discussed later.

Laser powers between 150 and 250 μJ with 10 ns pulses were used in this study, and the transitions are partially saturated. The fluorescence signal is collected over the (1,1) band near 314 nm. The fluorescence signal and laser power measurements are averaged over 300 laser pulses at each location, and corrections are made to the signal, which will be discussed later. To minimize the effects of collisional quenching on the OH signal, a short (5 ns), prompt detection gate on the fluorescence is used following the protocol described by Rensberger et al. (1989).

The experimental conditions were chosen to address all the questions posed earlier. Furthermore, high-purity gases are used at the inlet for combustion to keep surface contamination of substrates to a minimum. Three separate temperatures were selected for each of the substrate

materials to be tested. The first was the adiabatic temperature determined for each substrate from the temperature calibration step. These adiabatic temperatures range from 730 to 830 K, depending on substrate type and surface treatment. Experiments are run within a few degrees Kelvin of this calibrated adiabatic wall temperature to attempt to isolate the effect of surface temperature and composition, from the effect of heat flux at the substrate wall on the OH density in the combustion gases. Two additional higher temperatures (923 and 1123 K of the bottom TC) were also chosen to investigate the effect of higher substrate temperatures. Table 1 summarizes the results of the temperature calibration experiments.

The catalytic surface is prepared by e-beam evaporation of 1000 Å of Pt onto polished and unpolished Al₂O₃ backing discs. Each disc is cleaned using the standard RCA-1 (DI H₂O/H₂O₂/NH₄OH) and RCA-2 (DI H₂O/H₂O₂/HCl) cleaning procedures to remove organic and metallic contaminants, respectively. Preparation of the alumina substrates followed a procedure similar to that for the backing discs. One sample each from the polished and unpolished batches was annealed to possibly reduce the effect of surface defects and grain boundaries in the alumina on the quenching of the OH radical. The annealing schedule consisted of a 300°C/h ramp-up to a maximum of 1500°C. The substrates were held at 1500°C for 1 h and then cooled to room temperature at the rate of 300°C/h. Two SiO₂ substrates were also tested. The quartz substrates were cleaned using the previously outlined procedure. One of the two quartz samples was also annealed. The annealing schedule for the SiO₂ substrates was slightly different. These were heated to a maximum of 1100°C and held for 1 h. The ramp-up and ramp-down rates were lowered to 200°C/h to reduce thermal shock.

Samples were mounted in a specially designed ceramic holder (Figure 1) to avoid cracking and breaking of the holder during combustion and high-temperature operation. The holders are also cleaned using

Table 1. Summary of temperature calibration results

Substrate material	Line fit equation ^a	Adiabatic temperature (K)
Platinum	$T^{\text{Top}} = 0.845 T^{\text{Bottom}} + 113.5$	734
Alumina	$T^{\text{Top}} = 0.768 T^{\text{Bottom}} + 169.3$	729
Silica (quartz)	$T^{\text{Top}} = 0.725 T^{\text{Bottom}} + 228.2$	830

^aThe temperature are obtained within $\pm 5^\circ\text{C}$.

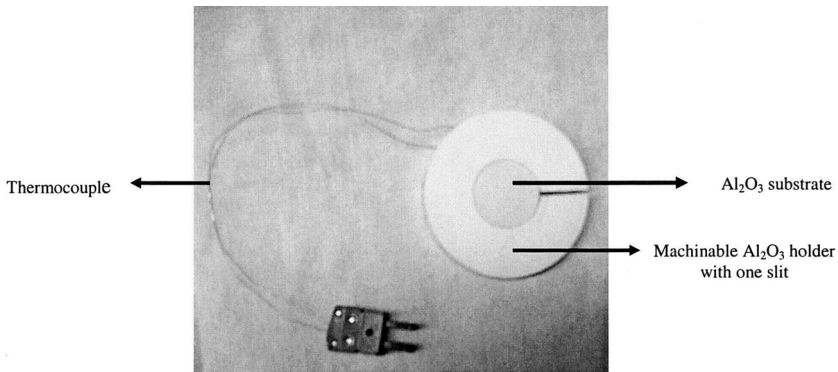


Figure 1. Al_2O_3 substrate mounted in a machinable alumina holder with one slit to reduce thermal stresses due to heating and cooling during experimentation.

the RCA-1 and RCA-2 procedures. The substrates are then glued from the back into the holder using Cotronics 989 high-temperature ceramic adhesive. A type-K thermocouple is also attached to the back using the same adhesive. The combustion chamber is pumped down to 20 Torr and is backfilled with N_2 while maintaining a 2 slm flow of the gas. After pressure stabilization, the substrate is baked out with O_2 flowing at 400°C for a half-hour followed by a reducing atmosphere bake-out with H_2 flowing at the same temperature. Next, the flame is started using a resistive igniter and acetylene gas to allow for quick ignition. The acetylene flow is slowly turned off and hydrogen flow is turned on until the desired stoichiometry and flow rates are achieved. The H_2/O_2 flame is allowed to run for 30 min before beginning any experiments. The temperature is then set to the desired value and allowed to reach steady state. For the current work, steady state has been defined as less than a 5°C change in temperature over a time period of 30 min. The thermocouple output is used as a feedback mechanism to control the power input to the substrate heater.

Information on laser measurements, details on beam alignment, and location of beam with respect to the substrate can be found in the work by Khadiya and Glumac (2000).

Modeling and Analysis Methodology

The Sandia National Laboratories CHEMKIN package was used for numerical computations. The specific program used was SPIN (Coltrin

et al., 1996). Details on the formulation and execution of the model can be found in the CHEMKIN user manuals (Kee et al., 1989). Two important aspects of the theoretical predictions are the gas-phase and surface-chemistry mechanisms. The gas-phase and surface reaction mechanisms along with the thermochemical and thermodynamic data for the various species as a function of temperature were obtained from literature (Gudmundson et al., 1998; Ikeda et al., 1995; Khadiya and Glumac, 2000; Miller and Bowman, 1989; Warnatz et al., 1994).

The model uses a full multi-component approach toward transport property calculations and takes into account the effect of thermal diffusion. The specified boundary conditions include the inlet velocity, burner temperature, and substrate temperature. To approximate near-zero recombination rates in the SPIN code when modeling inert surfaces, the rates of all surface reactions are multiplied by a scaling factor of 10^{-7} . The changes in the predicted OH profiles using the SPIN code are small for scaling factors less than 10^{-5} .

The LIF data were collected using a digital oscilloscope. Two voltages, one from the OH LIF signal and the other due to the laser power, were recorded. The LIF signal is converted to a number proportional to the OH number density using a series of corrections and transformations that account for various parameters, both physical and phenomenological, affecting the LIF signal. Discussion of each of the corrections and transformations follows. The LIF and laser power data are recorded at 18 locations in the 20 mm gap, beginning at the substrate wall, for each substrate temperature.

To ensure that the LIF signal is not affected by a location-dependent occlusion of the fluorescence by the substrate or the burner, a mask has been used on the collection optics that blocks half of the aperture. When taking measurements near the substrate, the lower half of the lens is blocked and near the burner the upper half is blocked. At the center of the gap, measurements are made with both mask orientations to allow for a compensation for the slight variation in collection efficiency due to mask orientation.

In keeping with other common data analysis techniques used in similar experiments, the LIF signal is corrected for a non-resonant background signal, variations in laser power, and laser drift as a function of time (Khadiya and Glumac, 2000; Rensberger et al., 1989).

The signal is also corrected for a changing Boltzmann fraction (f_B) with temperature in the flame. We choose a level ($F_2(6)$) that has a fairly

constant f_B in this temperature range, and we use the predicted temperature profile from the SPIN code to generate the quantitative value of f_B at each spatial location. The magnitude of this correction is less than 10%.

To convert the LIF signal into an OH number density, a calibration was performed using SPIN simulation values for OH concentrations predicted for the given combustion process. A multiplicative factor was obtained to convert the corrected LIF signal to a number density for each experimental case by scaling the maximum value for OH predicted by the SPIN model to the maximum value found in the LIF data. The same multiplicative factor is not used for each case but is determined based on the SPIN simulation results for that particular case. A representative plot in Figure 2 shows the scaling between the SPIN model and the LIF experimental results.

Due to limitations of the current experimental apparatus, scattering of light from the substrates, and the finite size of the laser beam, the closest LIF measurements placed the centroid of the laser beam 0.762 mm from the substrate surface. The gradient at this location is found using a

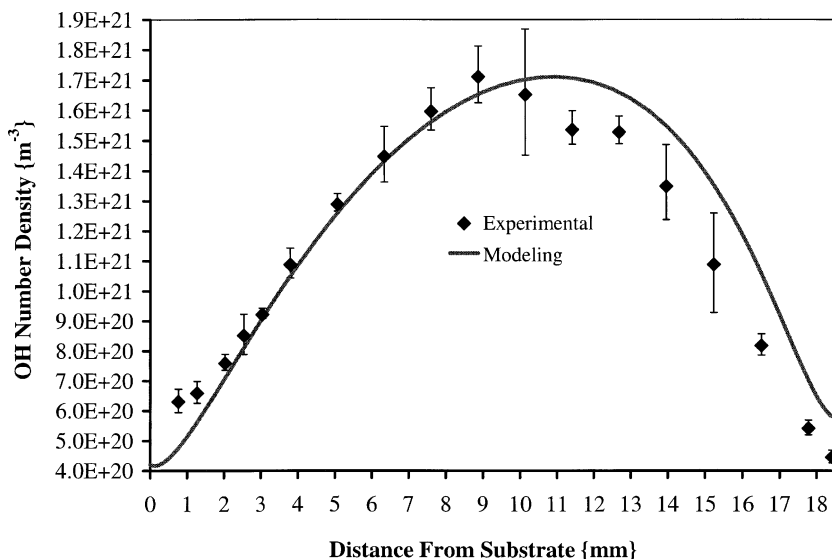


Figure 2. A representative plot showing comparison between the experimental and modeling values of OH radical number density as a function of distance from the SiO_2 substrate at 830 K. Flame conditions were $P = 20$ Torr and $\phi = 1$. Multiplicative factor obtained from the model is 4.85×10^{18} .

lowest-order polynomial curve fit for each of the test cases in the region several millimeters out from the substrate.

RESULTS AND DISCUSSION

To illustrate the effect of the surface composition and state on the OH radical concentration in the post-flame region of the hydrogen and oxygen stagnation flow combustor, Figure 2 shows a representative OH number density profile over a silica target with a surface temperature of 830 K. As seen in Figure 2, the OH number density, determined from the LIF data as described earlier, increases from a non-zero value near the silica substrate wall, reaches a peak, and then decays again toward the burner. Furthermore, the experimental LIF data show a lower number density from that predicted by the SPIN model nearest the burner. In particular for this investigation, the SPIN model also predicts a lower OH concentration from that determined by LIF nearest the substrate wall. In addition, it is observed that the maximum value of the OH concentration predicted from the SPIN model is located about 1–2.5 mm downstream compared to the peak location observed in the experiments. The explicit effect of the surface composition on the OH profile will be discussed in depth later, after first considering several issues that affect the reduction of the data.

The overall observations of the OH profile in Figure 2 are consistent with those seen by Khadiya and Glumac (2000) and Glumac (1997), when the differences between the physical apparatus and the assumptions underlying the model have been considered. One way to deal with the shifted flame front is to use a McKenna burner, but even this type of flat-flame burner has non-uniformities at the surface, and porous burners are generally not suitable for use in high-flux environments with high flow rate stagnation point flames over nearby high-temperature substrates. The shifted maximum peak in the model for the OH concentration can be explained by closely analyzing the burner inlet conditions. The model assumes a uniform flow across the burner face, with the flame stabilized at the burner face. In reality, the burner face is an array of 220 holes of diameter 0.75 mm drilled 2 mm apart in a 60 mm plate. Thus, the inlet gases emerging from the holes behave as a collection of jets, each undergoing an approximately conical expansion. The actual position where the flame stabilizes to a flat velocity front is not at the face of the burner but a few millimeters away due to the local

acceleration undergone by the expanding jets. Estimates on the lower and upper bounds for the shift in the distance that the peak occurs is obtained with a method similar to the analysis presented by Glumac (1997) in the work done with acetylene flames. For this work, the distance it takes for gases to expand into each other from one hole to another by diffusion is about 1.2 mm, and the condition of self-preservation of jets for five orifice diameters given by Tennekes and Lumley (1972) yields a maximum distance of 3.75 mm. Thus, the peak predicted by the SPIN model corrected by these bounds from the 20 mm physical distance is consistent with observed LIF peaks between 16.25 and 18.8 mm from the substrate.

An uncertainty analysis was conducted for the experimentally determined values for the OH concentration and gradient. Several data points were recorded at each location in the gap region between the substrate and the burner walls. A standard deviation, σ , for each data set was calculated at each location. The error due to the Boltzmann fraction correction was also included and added to the empirical uncertainty by the Kline–McClintock method. The error bars in Figure 2 show a 2σ variation for each point and include all uncertainties, as outlined earlier. The maximum uncertainty reported here is approximately 16%. For some data, uncertainty values were found to be as low as 2.4%. One caveat with respect to the uncertainty analysis is that it does not account for any errors introduced due to the conversion to OH number density using SPIN calculations. The uncertainty in the OH gradient was found from the standard error of the lowest-order regression fit of all the data points and directly adding to it the standard deviation found at each location, because these uncertainties are not assumed to be independent.

The effect of surface composition and temperature will be considered next by taking a closer look at the data in the following figures and tables. Figure 3 shows a plot comparing the OH number density for post-flame gases impinging on different types of Pt films on $\alpha\text{-Al}_2\text{O}_3$ backing plates: one with Pt directly applied on an unpolished plate from the manufacturer and the other having been polished before the Pt was applied. Figure 4 shows a comparison between different types of quartz substrates and Figures 5 and 6 show a similar comparison between the alumina substrates. Table 2 collates key data for all the cases near the wall.

For the Pt surfaces, as seen in Figure 3, both cases appear to have similar behavior, with a slight increase in OH number density with increase in surface temperature. As listed in Table 2, the gradient at

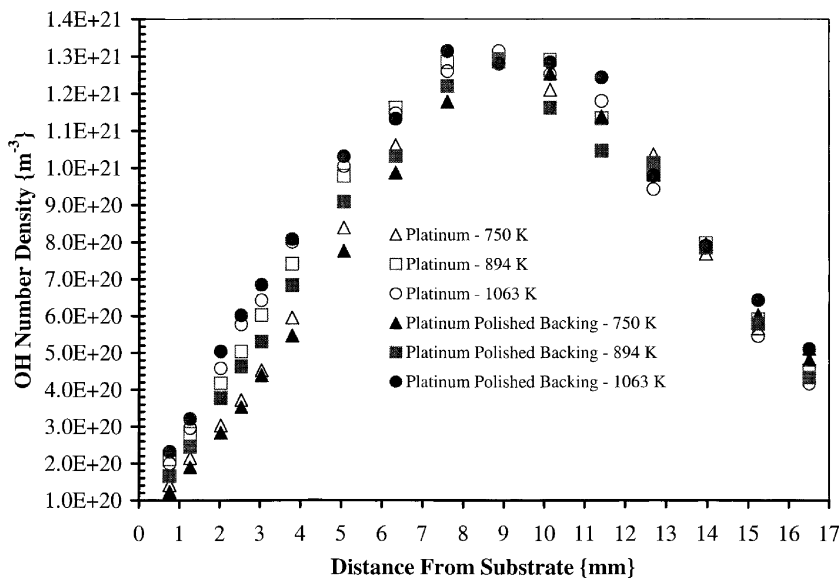


Figure 3. A comparative plot showing the OH radical concentration profile for different types of Pt films as a function of surface temperature. Flame conditions were $P = 20$ Torr Torr and $\phi = 1$. Error bars and modeling data curves are omitted for clarity, but they are of the same order as shown in Figure 2.

0.76 mm from the wall for Pt surface increases by about 38% and 26% for the polished and unpolished samples, respectively, with the increase in temperature from 750 to 1063 K. The OH number density for these cases similarly changes for these wall temperatures by approximately 16% and 13% for the polished and unpolished cases, respectively. The SiO_2 surfaces (see Figure 4) show an overall behavior similar to the Pt surfaces, except that the overall OH number density shows a much larger spread with temperature and surface preparation than Pt ($\sim 5 \times 10^{20}$ vs. $1 \times 10^{20} \text{ m}^{-3}$) at 0.76 mm from the wall. As seen from Table 2, the OH concentration is from 1.5 to about 7 times larger for the quartz than for Pt. The quartz surfaces, however, exhibit very similar gradients in OH concentration near the surface, with either no change or a slight decline with change in temperature from 830 to 1042 K, whereas for Pt two- to three-fold increases were observed. Overall, for the quartz surfaces, the absolute value for the OH gradient and concentration were often intermediate to those for the alumina and Pt surfaces. As will be

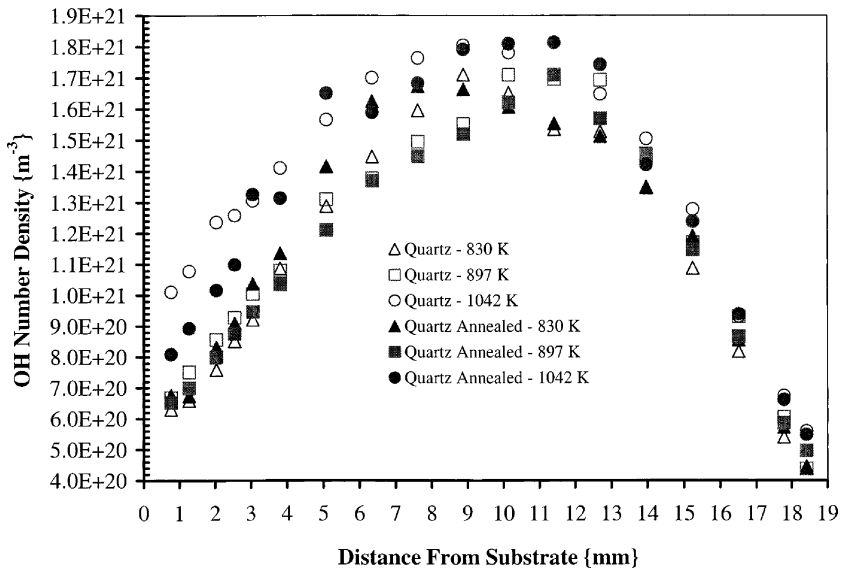


Figure 4. A comparative plot showing the OH radical concentration profile for different types of SiO_2 substrates as a function of surface temperature. Flame conditions were $P = 20$ Torr and $\phi = 1$. Error bars and modeling data curves are omitted for clarity, but they are of the same order as shown in Figure 2.

shown later, these differences in both gradient and concentration between the surface materials are significant.

As shown in Figures 5 and 6, the alumina surfaces, although similar to the quartz samples, have a more complex and different behavior with respect to temperature and surface conditioning. First, while the lowest OH number densities ($\sim 9 \times 10^{20} \text{ m}^{-3}$) are approximately the same as the quartz, there is a wider spread (~ 1.3 times greater) in concentration with increase in temperature for the alumina than the quartz, and much wider (~ 8 times greater) than for Pt. More importantly, compared to the Pt and SiO_2 surfaces, the OH gradient is smaller by up to an order of magnitude for the alumina surfaces. Also, upon close examination of Figures 5 and 6, there also appears to be differences in OH profile due to surface preparation (such as as-formed, polished, and annealed) that were not observed for the quartz or Pt. It appears that various surface preparation schemes such as polishing and annealing introduce changes in the fine microstructure of the materials. For instance, polishing cuts new faces in the crystalline material exposing different crystal orientations to the

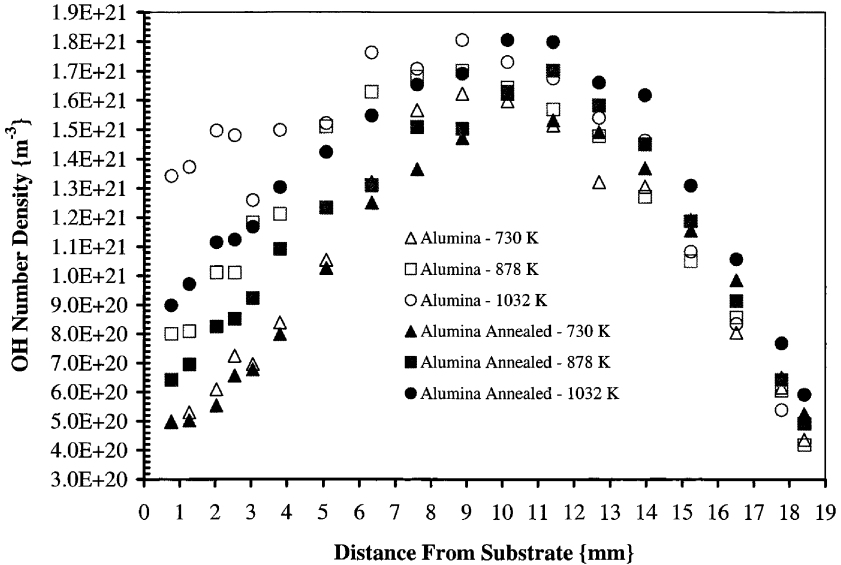


Figure 5. A comparative plot showing the OH radical concentration profile for different types of Al_2O_3 substrates as purchased from the manufacturer as a function of surface temperature. Flame conditions were $P = 20$ Torr and $\phi = 1$. Error bars and modeling data curves are omitted for clarity, but they are of the same order as shown in Figure 2.

gases and thus potentially introducing variations in radical quenching rates due to different absorption or recombination of OH on different crystal planes.

The data and uncertainty estimates show that surface composition and material processing have a significant effect on the OH profile relatively far from the surface (from 0.76 to 10 mm) leading to some increased scatter in data on the burner side (near 16 to 20 mm from substrate; see Figures 5 and 6). It has been shown by Forsth et al. (1999) that the OH profile depends in a complex and coupled manner on several factors, such as the diffusion of OH from the substrate surface, convection currents away from the surface, changes in gas density due to the temperature distribution in the gases, and gas-phase reactions in flames over 5 Torr. The observed scatter on the burner side as a function of surface temperature is not large with respect to the uncertainty values presented above. A maximum uncertainty of 16% was found, not accounting for the calibration error as mentioned earlier. The calibration error could be as high as 20% or more in comparison to, for example, 11% difference in

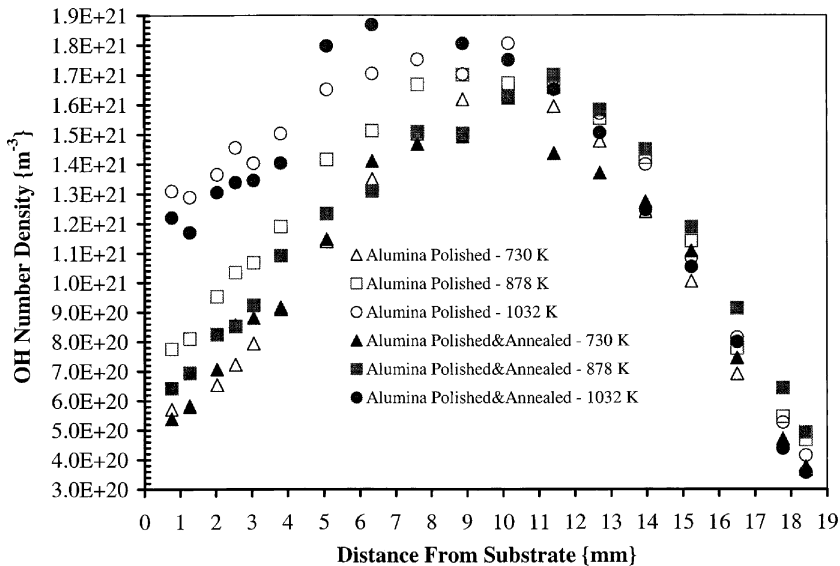


Figure 6. A comparative plot showing the OH radical concentration profile for different types of polished Al_2O_3 substrates as a function of surface temperature. Flame conditions were $P = 20$ Torr and $\phi = 1$. Error bars and modeling data curves are omitted for clarity, but they are of the same order as shown in Figure 2.

the OH number density at 18.415 mm from the substrate at 1032 K for the two types of polished alumina walls. Our hypothesis is that the wall composition, local morphology, and temperature have a strong coupled action on the destruction of OH at the wall, which in turn affects the OH profile in the post-flame region. It appears from Figures 3–6 and Table 2 that two major components that illustrate the action that a surface has on the chemical recombination or destruction of the OH radical are the gradient and the number density of the hydroxyl radical near the surface of interest. However, when comparing Figure 3 to Figures 4 and 5, and Figure 5 to Figure 6, it also appears that neither concentration (C) nor the slope by themselves fully characterize the effect of the surface on the overall OH concentration profile. A quantity that captures the effect of the surface would be a useful tool in analyzing the behavior of the substrate walls toward OH destruction.

Chemical action, A , refers to any chemical process determined by the atomic and molecular composition and structure of the substances involved. The non-dimensional action A for the effect that the surface

Table 2. Effect of surface conditions and temperatures on hydroxyl radical (OH) gradient and number density at 0.76 mm from the substrate wall

Substrate material	Surface temperature (K)	Surface condition	OH gradient (m ⁻³ /mm)	OH number density (#/m ³)
Platinum	750	Polished	$1.3 \times 10^{20} \pm 2.4 \times 10^{19}$	$1.2 \times 10^{20} \pm 7.7 \times 10^{18}$
		Unpolished	$1.5 \times 10^{20} \pm 2.4 \times 10^{19}$	$1.4 \times 10^{20} \pm 9.0 \times 10^{18}$
	1063	Polished	$1.8 \times 10^{20} \pm 2.7 \times 10^{18}$	$2.3 \times 10^{20} \pm 1.5 \times 10^{19}$
		Unpolished	$1.9 \times 10^{20} \pm 2.8 \times 10^{18}$	$2.0 \times 10^{20} \pm 1.3 \times 10^{19}$
Silica (quartz)	830	Annealed	$2.0 \times 10^{20} \pm 3.0 \times 10^{19}$	$5.0 \times 10^{20} \pm 3.2 \times 10^{19}$
		Unannealed	$2.0 \times 10^{20} \pm 3.0 \times 10^{19}$	$5.0 \times 10^{20} \pm 3.2 \times 10^{19}$
	1042	Annealed	$2.0 \times 10^{20} \pm 3.0 \times 10^{19}$	$7.0 \times 10^{20} \pm 4.5 \times 10^{19}$
		Unannealed	$1.0 \times 10^{20} \pm 2.7 \times 10^{19}$	$9.0 \times 10^{20} \pm 5.8 \times 10^{19}$
Alumina	730	Annealed	$2.1 \times 10^{20} \pm 5.1 \times 10^{19}$	$9.2 \times 10^{20} \pm 5.9 \times 10^{19}$
		Unannealed	$2.1 \times 10^{20} \pm 5.5 \times 10^{19}$	$9.4 \times 10^{20} \pm 6.0 \times 10^{19}$
		Polished	$2.1 \times 10^{20} \pm 5.8 \times 10^{19}$	$1.1 \times 10^{21} \pm 7.0 \times 10^{19}$
		Polished & annealed	$3.8 \times 10^{20} \pm 5.3 \times 10^{19}$	$1.0 \times 10^{21} \pm 6.4 \times 10^{19}$
	1032	Annealed	$2.9 \times 10^{20} \pm 4.3 \times 10^{19}$	$1.5 \times 10^{21} \pm 9.6 \times 10^{19}$
		Unannealed	$5.8 \times 10^{19} \pm 3.9 \times 10^{19}$	$2.3 \times 10^{21} \pm 1.5 \times 10^{20}$
		Polished	$1.9 \times 10^{20} \pm 4.0 \times 10^{19}$	$2.2 \times 10^{21} \pm 1.4 \times 10^{20}$
		Polished & annealed	$2.0 \times 10^{20} \pm 4.4 \times 10^{19}$	$1.9 \times 10^{21} \pm 1.2 \times 10^{20}$

has on the OH concentration profile is defined in this paper as the ratio of the gradient of the OH radical concentration to the number density of the OH radical at the position of interest. It appears to be a more sensitive measure than either C or the slope in C , particularly when concentration near the wall is small compared to that far from the wall. It is non-dimensionalized by using a characteristic length, L_c , for the system that corresponds to half the distance between the substrate wall and the burner wall, i.e.

$$A = \left(\frac{\partial C_{\text{OH}} / \partial \hat{x}}{C_{\text{OH}}} \right)_{\text{Location}, l}, \quad \hat{x} = \frac{x}{L_c} \quad (1)$$

The action A as defined by Eq. (1) depends in a complicated manner on both gas-phase reaction rates and surface reactions, as well as transport of the OH radical at the location of interest. The use of the near-surface gradient has also been used by Khadiya and Glumac (2000) to test the predictions of the surface chemistry models. The lower the action

that the surface has on the combustion process, the lower the destruction rate, or conversely the higher the generation rate, of OH is near or at the surface, with respect to the concentration of OH in the gases.

To illustrate the use of this defined chemical action, Figure 7 shows a comparison between the measured A and the predicted value obtained from SPIN calculations at 0.762 mm from the substrate wall. As can be seen from Figure 7, the predicted trend and values agree within 7% at 750 K and within 1% at the higher temperatures with the experimental results obtained for the Pt substrate. Due to the lack of detailed surface chemistry models for the Al_2O_3 and SiO_2 substrates, accurate predictions cannot be made for these materials. However, considering Pt as a reference, it is evident from Figure 7 that the action for Al_2O_3 and SiO_2 is lower by one to nearly two orders of magnitude than the Pt surfaces, and that the experimental trends displayed for the two materials also show different behavior in comparison to each other.

Figure 7 shows that the action for all the alumina data drops from 0.002 by an order of magnitude as the surface temperature increases from

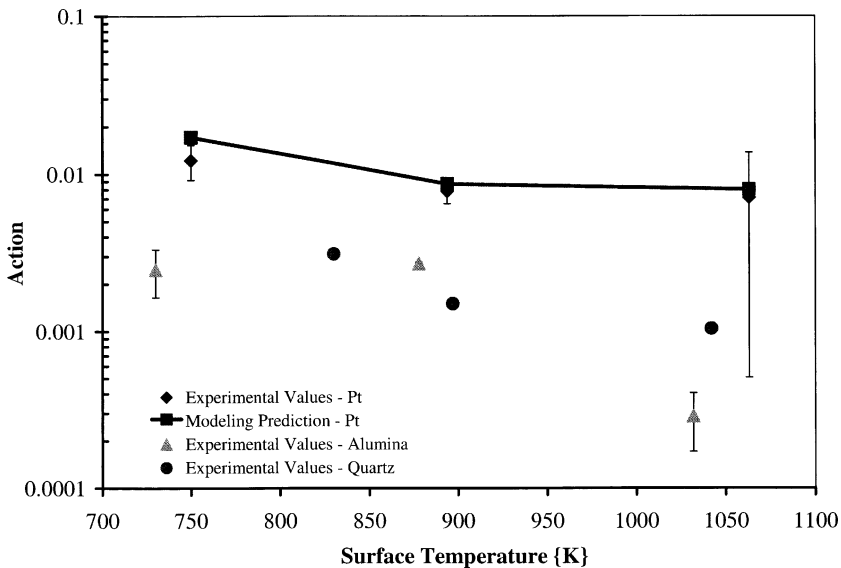
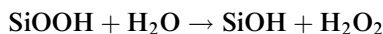
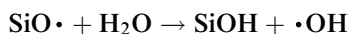


Figure 7. The plot shows non-dimensional chemical action as a function of surface temperature at 0.762 mm from the substrate wall. The chemical action is non-dimensionalized by using a characteristic length for the system that corresponds to half the distance between the substrate wall and the burner wall. Flame conditions were $P = 20$ Torr and $\phi = 1$.

730 K to about 1050 K at 0.762 mm from the wall. For the same change in temperature, the action for silica changes by about three-fold. Furthermore, in the same temperature range, alumina displays an apparent inverted-V trend and silica shows a trend nearly opposite that of alumina for the values of A determined experimentally. It is difficult to determine if the inverted trend exists at all temperatures from the few temperatures that were tested; both materials, however, show statistically significant reductions in action over Pt. The difference in behavior of alumina and silica on OH concentration can also be seen in Figures 4–6. For instance, at 0.762 mm from the alumina wall at 1032 K, the number density is approximately $2.3 \times 10^{21} \text{ m}^{-3}$ and for quartz at 1042 K at the same location the value is $9.0 \times 10^{20} \text{ m}^{-3}$, but the gradient for the alumina wall is almost an order of magnitude lower. It would appear that for both alumina and silica there are surface reactions taking place that affect the OH profiles in the gas phase near the substrate wall. These reactions, though, are not yet fully understood, making the task of predicting the exact behavior of these surfaces toward OH radical recombination difficult and emphasizing the need for better surface-chemistry models.

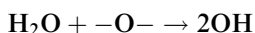
The literature is relatively sparse and exact surface reaction mechanisms for OH recombination and generation on alumina and silica are not as readily available as they are for Pt; there is some evidence that OH may not be absorbed at alumina and silica surfaces and that OH may be produced at surfaces containing bound oxygen by reaction with water under some circumstances. From the OH LIF profiles, the sticking coefficients of various radical species on the walls cannot be accurately estimated, thus making it difficult to quantify the behavior of alumina and quartz to radicals such as O, H, and their relation to the yield of water. Several researchers have shown that, in the presence of water at elevated temperatures, both crystalline and amorphous silica surfaces react with water to form stable hydroxyl-terminated silanol groups (Davis and Tomozawa, 1995, 1996; Doremus, 1999; Konecny, 2001). Pfefferle et al. (1988) have shown that some radical recombination is known to occur on fused-silica substrates. Kirchoff and Braun (1992) showed the formation of OH radical during the processing of quartz tubes with oxy-hydrogen burners. Shi et al. (1995) have suggested the generation of active oxygen by quartz particles. The presence of active oxygen with water at elevated temperatures may lead to gas-phase generation of OH radicals. Indeed, the reaction of water with silica at elevated temperatures is well known to dramatically increase oxidation rates of sili-

con, through reactions involving OH. Konecny (2001) suggested some chemical reactions that may occur on quartz surfaces:



The silanol groups formed are a stable species and have a high surface density. The reaction of these stable silanol groups with the OH radical is likely to result in the rejection of the radical back into the gas-phase. Konecny (2001) has also suggested that OH may be produced on silanol-terminated surfaces to a much lesser extent. The mechanism presented in the paper by Miller and Bowman (1989) shows the importance of H₂O₂ in generating OH and another important radical, HO₂, that may aid in the generation of more OH radicals.

There is a large amount of ongoing research in understanding the surface interactions of metal oxides with water (Goniakowski and Gillan, 1996; Hass et al., 1998, 2000; Manassidis et al., 1993; Nygren et al., 1997; Trout and Parrinello, 1998; Verdozi et al., 1999). Hass et al. (2000) stated that Al₂O₃ is one of the most common and yet least understood metal oxides. Through molecular dynamic simulations, Hass et al. (2000) have suggested that OH and H₂O may be present on the surface of α -Al₂O₃ with high density. Doremus (1999) suggested that oxygen-bound crystalline compounds may react with water molecules at elevated temperatures (>500°C) through a complicated diffusion-reaction mechanism that yields



Hass et al. (2000) have also suggested that on the surface of α -Al₂O₃ a high density of complex and different structural forms of alumina may be present. Furthermore, the presence of some of these forms may assist in water-mediated dissociation events. Depending on the form present at the surface, α -Al₂O₃ may be more inert and could possibly even assist in generating the OH radical and thus perform better than SiO₂ with respect to lower recombination of the hydroxyl radical. With a lower OH destruction rate, or potentially even a net OH generation rate, for α -Al₂O₃ and quartz surfaces, the transport of OH from the flame region to the surfaces, and concentration of OH in the gases above the surfaces, is expected to be higher than that for Pt. These trends appear to be

confirmed by the experimental OH profiles (Figures 3–6) and a comparison of the calculated values of A (Figure 7). Clearly, further work is needed to clarify the reactions at the surfaces of these oxides to accurately predict the action of the surface on the gas-phase concentrations of OH.

CONCLUSIONS AND FUTURE WORK

Of the three surface materials tested under various conditions, it was found that Pt produced the lowest OH concentration in the gases above the surface, whereas Al_2O_3 provided the highest level of OH concentration at higher temperatures. The effect of a quartz surface on OH concentration lies between that of Pt and Al_2O_3 . One of the important conclusions of the present work is the quantitative difference in behavior of the quartz and alumina; to the knowledge of the authors, no such distinction has been made in the literature with respect to radical quenching on substrate walls made of these materials. A more detailed surface study quantifying the effect of modifying the surface through annealing and polishing is needed. Furthermore, to accurately predict the OH profile above the surface, detailed surface chemistry models are needed for alumina and silica, similar to that for Pt surfaces. However, the main purpose of this research was to provide evidence that materials traditionally considered inert, such as α -alumina and quartz, do act at high temperatures to increase OH radical concentrations in the gases over a known reactive material, Pt.

REFERENCES

- Aghalayam, P., Bui, P.-A., and Vlachos, D.G. (1998) The role of radical wall quenching in flame stability and wall heat flux: Hydrogen–air mixtures. *Combust. Theor. Model.*, **2**, 515.
- Balat, M., Czerniak, M., and Badie, J.M. (1997) Thermal and chemical approaches for oxygen catalytic recombination evaluation on ceramic materials at high temperature. *Appl. Surf. Sci.*, **120**, 225.
- Cotrin, M.E., Kee, R.J., Evans, G.H., Meeks, E., Rupley, F.M., and Grcar, J.F. (1996). A fortran program for modelling one-dimensional rotating-disk/stagnation-flow chemical vapour deposition reactors. Technical Report SAND 91-8003, Sandia National Laboratories.
- Daily, J.W. (1997) Laser induced fluorescence spectroscopy in flames. *Prog. Energy Combust. Sci.*, **23**, 133.

- Davis, K.M. and Tomozawa, M. (1995) Water diffusion into silica glass: Structural changes in silica glass and their effect on water solubility and diffusivity. *J. Non-cryst. Solids*, **185**, 203.
- Davis, K.M. and Tomozawa, M. (1996) An infrared spectroscopic study of water-related species in silica glasses. *J. Non-cryst. Solids*, **201**, 177.
- Deutschmann, O., Schmidt, R., Behrendt, F., and Warnatz, J. (1996) Numerical modeling of catalytic Ignition, *Proc. Combust. Instit.*, **26**, 1747.
- Doremus, R.H. (1999) Diffusion of water in crystalline and glassy-oxides: Diffusion-reaction model. *J. Mater. Res.*, **15**, 3754.
- Fernandez-Pello, A.C. (2002) Micro-power generation using combustion: Issues and approaches. *Proc. Combust. Instit.*, **29**, 883.
- Forsth, M., Gudmundson, F., Persson, J., and Rosen, A. (1999) The influence of a catalytic surface on the gas-phase combustion of $\text{H}_2 + \text{O}_2$. *Combust. Flame*, **119**, 144.
- Fridell, E. and Rosen, A. (1994) A laser-induced fluorescence study of OH desorption from Pt in $\text{H}_2\text{O}/\text{O}_2$ and $\text{H}_2\text{O}/\text{H}_2$ mixtures. *Langmuir*, **10**, 699.
- Glumac, N.G. (1997) Flame temperature predictions and comparison with experiment in high flow rate, fuel-rich acetylene/oxygen flames. *Combust. Sci. Technol.*, **122**, 383.
- Goniakowski, J. and Gillan, M.J. (1996) The adsorption of H_2O on TiO_2 and $\text{SnO}_2(110)$ studied by first-principles calculations. *Surf. Sci.*, **350**, 145.
- Gudmundson, G., Persson, J., Forsth, M., Behrendt, F., Kasemo, B., and Rosen, A. (1998) OH gas phase chemistry outside a Pt catalyst. *J. Catal.*, **179**, 420.
- Hahn, D.W., Edwards, C.F., McCarty, K.F., and Kee, R.J. (1996) Large-area diamond deposition in an atmospheric pressure stagnation-flow reactor. *Appl. Phys. Lett.*, **68**, 2158.
- Hass, K.C., Schneider, W.F., Curioni, A., and Andreoni, W. (1998) The chemistry of water on alumina surfaces: Reaction dynamics from first principles. *Science*, **282**, 265.
- Hass, K.C., Schneider, W.F., Curioni, A., and Andreoni, W. (2000) First-principles molecular dynamics simulations of H_2O on $\alpha\text{-Al}_2\text{O}_3$ (0001). *J. Phys. Chem. B*, **104**, 5527.
- Ikedda, H., Sato, J., and Williams, F. (1995) Surface kinetics for catalytic combustion of hydrogen-air mixtures on platinum at atmospheric pressure in stagnation flows. *Surf. Sci.*, **326**, 11.
- Kee, R.J., Rupley, F.M., Miller, J.A., Evans, G.H., Meeks, E., and Grcar, J.F. (1989) *CHEMKIN-II: A FORTRAN Chemical Kinetics Package for Analysis of Gas-Phase Chemical Kinetics*. Technical Report SAND89-8009, Sandia National Laboratories.
- Kelley, S.C., Deluga, G.A., and Smyrl, W.H. (2002) Miniature fuel cells fabricated on silicon substrates. *AIChE J.*, **48**, 1071.

- Khadiya, N. and Glumac, N.G. (2000) Validation of surface chemistry models using low pressure stagnation-point flames: Measurements of OH above platinum surfaces. *Combust. Sci. Technol.*, **159**, 147.
- Kirchoff, J. and Braun, G. (1992) Hydroxyl formation in silica tubes and layers due to oxy-hydrogen flames. *Mat. Res. Soc. Symp. Proc.*, **244**, 15.
- Konecny, R. (2001) Hydroxyl reactivity of hydroxyl radicals on hydroxylated surface. 1. Cluster model calculations. *J. Phys. Chem. B*, **105**, 6221.
- Kuo, K.-Y. (1986) Principles of Combustion, Wiley, New York, p. 326.
- Kurkov, A.P. and Mirsky, W. (1968) An Analysis of the Mechanism of Flame Extinction by a Cold Wall. *Proc. Combust. Instit.*, **12**, 615.
- Kyritsis, D.C., Guerrero-Arias, I., Roychoudhury, S., and Gomez, A. (2002) Mesoscale Power Generation by a Catalytic Combustor Using Electro-sprayed Liquid Hydrocarbons. *Proc. Combust. Instit.*, **29**, 965.
- Laurendeau, N.M. and Goldsmith, J.E.M. (1989) Comparison of hydroxyl concentration profiles using five laser-induced fluorescence methods in a lean subatmospheric-pressure H₂/O₂/Ar flame. *Combust. Sci. Technol.*, **63**, 139.
- Ljungström, S., Hall, J., Kasemo, B., Rosen, A., and Wahnström, T. (1987) A comparative study of OH radical desorption in the H₂ + O₂ reaction on Pt, Pd, Rh, Ir, and Ni. *Journal of Catalysis*, **107**, 548.
- Manassidis, I., De Vita, A., and Gillan, M.J. (1993) Structure of the (0001) surface of α -Al₂O₃ from first principles. *Surf. Sci.*, **285**, L517.
- Mardsen, D.G.H. and Linnett, J.W. (1955) Recombination of oxygen atoms on surfaces. *Proc. Combust. Instit.*, **5**, 685.
- Masel, R.I. and Shannon, M.A. (2001) *Microcombustor Having Submillimeter Critical Dimensions*. U.S. Patent 6,193,501.
- Miese, C.M., Jensen, C.J., Masel, R.I., Shannon, M.A., and Short, M. (2004) Sub-millimeter scale combustion. *AIChE J.*, **50**, 3206.
- Miese, C.M., Masel, R.I., Short, M., and Shannon, M.A. (2004) Diffusion Flame Instabilities in a 0.75 mm Non-premixed burner. *Proc. Combust. Instit.*, **30**.
- Miller, J.A. and Bowman, C.T. (1989) Mechanism and modeling of nitrogen chemistry in combustion. *Prog. Energy Combust. Sci.*, **15**, 287.
- Nygren, M.A., Gay, D.H., and Catlow, C.R.A. (1997) Hydroxylation of the surface of the corundum basal plane. *Surf. Sci.*, **380**, 113.
- Pfefferle, L.D., Griffin, T.A., and Winter, M. (1988) Planer laser-induced fluorescence of OH in a chemically reacting boundary layer. *Appl. Opt.*, **27**, 3197.
- Raimondeau, S., Norton, D., Vlachos, D.G., and Masel, R.I. (2002) Modeling of High-Temperature Microburners. *Proc. Combust. Instit.*, **29**, 901.
- Reineke, M., Mantzaras, J., Schaeren, R., Bombach, R., Kreutner, W., and Inauen, A. (2002) Homogeneous ignition in High-Pressure Combustion of Methane/Air over Platinum: Comparison of Measurements and Detailed Numerical Predictions. *Proc. Combust. Instit.*, **29**, 1021.

- Rensberger, K.J., Jeffries, J.B., Copeland, R.A., Kohse-Höinghaus, K., Wise, M.L., and Crosley, D.R. (1989) Laser-induced fluorescence determination of temperatures in low-pressure flames. *Appl. Opt.*, **28**, 3556.
- Schwiedernoch, R., Tischer, S., Deutschmann, O., and Warnatz, J. (2002) Experimental and Numerical Investigation of the Ignition of Methane Combustion in a Platinum-Coated Honeycomb Monolith. *Proc. Combust. Instit.*, **29**, 1005.
- Shi, X., Mao, Y., Daniel, L.M., Saffiotti, U., Dalal, N.S., and Vallyanthan, V. (1995) Generation of reactive oxygen species by quartz particles and its implication for cellular damage. *Appl. Occup. Environ. Hyg.*, **10**, 1138.
- Sidwell, R.W., Zhu, H., Kee, R.J., Wickham, D.T., Schell, C., and Jackson, G.S. (2002) Catalytic Combustion of Premixed Methane/Air on a Palladium-Substituted Hexaluminate Stagnation Surface. *Proc. Combust. Instit.*, **29**, 1013.
- Takeda, K., Ahn, J., Borer, K., Sitzki, L., Ronney, P.D., and Deutschmann, O. (2002) Extinction Limits of Catalytic Combustion in Microchannels. *Proc. Combust. Instit.*, **29**, 957.
- Tennekes, H. and Lumley, J.L. (1972) *A First Course in Turbulence*, MIT Press, Cambridge, Massachusetts.
- Trout, B.L. and Parrinello, M. (1998) The dissociation of H_2O in water studied by first-principles molecular dynamics. *Chem. Phys. Lett.*, **288**, 343.
- Verdozzi, C., Jennison, D.R., Schultz, P.A., and Sears, M.P. (1999) Sapphire (0001) surface, clean and with d-metal overlayers. *Phys. Rev. Lett.*, **82**, 799.
- Vican, J., Gajdeczko, B.F., Dryer, F.L., Milius, D.L., Aksay, I.A., and Yetter, R.A. (2002) Development of a Microreactor as a Thermal Source for Microelectromechanical Systems Power Generation. *Proc. Combust. Instit.*, **29**, 909.
- Warnatz, J., Allendorf, M.D., Kee, R.J., and Coltrin, M.E. (1994) A model of elementary chemistry and fluid mechanics in the combustion of hydrogen on platinum surfaces. *Combust. Flame*, **96**, 393.